THE ASTROPHYSICAL JOURNAL LETTERS, 1003:L30 (7pp), 2026 June 1 https://doi.org/10.3847/2041-8213/ae66e5

First Detection of HC_5N in a Class II Disk around TW Hya

Steven C. Wampler[1], Ryan A. Loomis[1], Amina Diop[2], L. Ilsedore Cleeves[2], Yuri Aikawa[3], Romane Le Gal[4], Viviana Guzman[5,6], Charles J. Law[2,10], Karin Oberg[7], Jamila Pegues[2], Richard Teague[8], and Catherine Walsh[9]
[1] National Radio Astronomy Observatory, Charlottesville, VA 22903, USA; swampler@nrao.edu
[2] Department of Astronomy, University of Virginia, Charlottesville, VA 22904, USA
[3] Department of Astronomy, Graduate School of Science, The University of Tokyo, Tokyo 113-0033, Japan
[4] Institut de Planétologie et d'Astrophysique de Grenoble, Institut de Radioastronomie Millimétrique, Université Grenoble Alpes, Saint-Martin-d'Héres, Auvergne Rhône-Alpes, France
[5] Institute of Astrophysics, Pontificia Universidad Católica de Chile, Vicuña Mackenna 4860, Macul, Región Metropolitana, Chile
[6] Millennium Nucleus on Young Exoplanets and their Moons (YEMS), Santiago, Chile
[7] Center for Astrophysics, Harvard & Smithsonian, 60 Garden St., Cambridge, MA 02138, USA
[8] Department of Earth, Atmospheric, and Planetary Sciences, Massachusetts Institute of Technology, Cambridge, MA 02139, USA
[9] School of Physics and Astronomy, University of Leeds, Leeds LS2 9JT, UK
Received 2026 January 30; revised 2026 April 20; accepted 2026 April 28; published 2026 May 20

Abstract

Over the last decade of ALMA's operation the molecular inventory of protoplanetary disks has expanded rapidly, revealing a diverse set of nitrogen-bearing organics and carbon-chain molecules that trace both prebiotic chemistry and fundamental disk physics. Despite this progress, detections of larger species such as cyanopolyynes have remained limited, leaving larger carbon-chain chemistry in Class II disks largely unconstrained. Here, we report the first detection of HC_5N toward the TW Hya protoplanetary disk, representing the largest cyanopolyyne identified to date in a Class II system. We derive a HC_5N column density for two rotational transitions $J = 41–40$ and $J = 37–36$ $N_T \sim 10^{12}$ cm^{-2} for assumed $T_{rot} = 20–50$ K and optically thin emission in LTE. We compare HC_5N and HC_3N formation mechanisms and analyze the HC_3N/HC_5N ratio. We use a chemical model to estimate the expected abundance and emitting layer of HC_5N in a TW Hya–like disk. Although HC_5N emission is spatially unresolved and measured column densities suggest an origin in the warm molecular layer where CN-based pathways are active. This detection extends the known carbon-chain chemistry in Class II disks and demonstrates that long cyanopolyynes can form and persist in planet-forming environments.

Unified Astronomy Thesaurus concepts: Protoplanetary disks (1300); Astrochemistry (75); Interstellar molecules (849); Molecular spectroscopy (2095); Millimeter astronomy (1061)

1. Introduction

Protoplanetary disks contain the molecular reservoirs that ultimately seed the formation of planets, moons, and comets. An increasing number of confirmed exoplanets is revealing a wide diversity of physical and chemical environments (e.g., R. L. Akeson et al. 2013), and with the advent of JWST, exoplanet atmospheres are now being characterized directly. Linking these atmospheric measurements to the chemical initial conditions of planet formation requires a detailed understanding of the molecular inventories present in disks. ALMA observations offer the opportunity to connect the disk chemistry of evolving stellar systems to the chemical inventories of mature planets. Understanding how disk chemistry evolves requires sampling systems across stellar masses and evolutionary stages, since molecular abundances and physical conditions vary substantially between young Class I disks, older Class II disks, and disks around T Tauri and Herbig Ae stars.

Complex organic molecules (COMs) are readily observed in the warm, dense regions surrounding Class 0 protostars (e.g., J. K. Jørgensen et al. 2016). Recent work has shown that COMs can accrete onto disks from the surrounding envelope and are present during the early stages of star formation (N. M. Murillo et al. 2022). COMs have also been detected in a small number of warmer, high-mass Herbig Ae disks (e.g., A. S. Booth et al. 2024, 2025, 2026; Y. Yamato et al. 2024). By contrast, detections of COMs in Class II T Tauri disks are exceedingly rare with only two species, CH_3OH (C. Walsh et al. 2016) and CH_3CN (K. I. Öberg et al. 2015), detected to date. This scarcity most likely reflects the extremely low gas-phase abundances of these COMs in disks, where they are readily destroyed, frozen out, or inefficiently produced (e.g., C. Walsh et al. 2014). What remains unclear then is the link between the chemically rich environments of young protostellar systems and their older and colder counterparts. The rarity of COM detections in T Tauri disks limits our ability to assess how much chemical complexity is inherited versus produced in situ, while observations of simpler species suggest that disk physical conditions, including variations in the C/O ratio, play a major role in regulating this chemistry (e.g., K. I. Öberg et al. 2011, 2015; J. B. Bergner et al. 2018; K. I. Öberg et al. 2023; Y. Aikawa et al. 2024).

While CH_3CN is the only nitrogen-bearing COM detected in Class II T Tauri disks to date, other smaller nitrile species, characterized by the presence of a cyano group (-CN), have emerged as critical probes for understanding the chemistry relevant to planet and comet formation. Measurements from the Rosetta mission revealed that nitriles are abundant in solar system comets (e.g., L. Le Roy et al. 2015), suggesting that

[10] NASA Hubble Fellowship Program Sagan Fellow.

they are critical to understanding the chemistry of the early solar nebula. Although large and complex nitrile species will likely undergo destruction during planet formation and on early Hadean-like exoplanet surfaces, the cyanide group itself can persist under these conditions (K. J. Zahnle 1986; M. W. Powner et al. 2009). Beyond their importance to prebiotic chemistry, the cyano functional group imparts a large dipole moment and hyperfine splitting, yielding multiple strong rotational transitions that are accessible within a single observation. These unique properties make them effective tracers of disk structure constraining elemental abundances, isotopic ratios both radially and vertically within disks, turbulence, and constraining magnetic fields. (e.g., V. V. Guzmán et al. 2017; J. B. Bergner et al. 2021; G. Cataldi et al. 2021; R. Teague et al. 2016; T. Paneque-Carreño et al. 2024; R. Teague et al. 2025)

Cyanopolyynes, which are long unsaturated carbon-chain nitriles of the form HC_nN where $n = 3,5,7\ldots$, are frequently detected in other interstellar environments including the envelopes of evolved stars and cold dark clouds (e.g., N. W. Broten et al. 1978), and their chemistry is largely understood to proceed via gas-phase reactions (e.g., K. Fukuzawa et al. 1998; K. Taniguchi et al. 2017). Their precursors CN, C_2H_2, and HCN have long been known to exist in disks (e.g., A. Dutrey et al. 1997; G.-J. van Zadelhoff et al. 2001; W.-F. Thi et al. 2004; E. L. Gibb et al. 2007; J. S. Carr & J. R. Najita 2008), but detections of larger HC_nN species have only been made in other environments, extending up to $HC_{11}N$ (e.g., R. A. Loomis et al. 2021). To date, HC_3N remains the only cyanopolyyne detected in a Class II disk (e.g., E. Chapillon et al. 2012; K. I. Öberg et al. 2015; J. B. Bergner et al. 2018; J. D. Ilee et al. 2021; N. T. Phuong et al. 2021). In the interstellar medium (ISM), cyanopolyynes serve as valuable tracers of both physical and chemical conditions, providing diagnostics of temperature, turbulence, and isotopic fractionation (e.g., K. Taniguchi et al. 2019). Their utility for isotopic studies arises from their carbon-chain structure, each molecule containing both multiple carbon atoms and a cyano functional group, allowing for constraints on carbon and nitrogen fractionation (e.g., N. Sakai et al. 2011; K. Taniguchi et al. 2017; A. M. Burkhardt et al. 2018). Cyanopolyynes also have large dipole moments that facilitate reliable determinations of column densities (N_T) and rotational temperatures ($T_{\rm rot}$) (e.g., A. Dutrey et al. 1997; J. H. Kastner et al. 1997; E. Chapillon et al. 2012; J. B. Bergner et al. 2018), and as the carbon-chain length increases, the rotational transitions become more closely spaced in frequency, enabling more efficient coverage within a single spectral setup for bandwidth-limited observations. These factors make detections of longer cyanopolyynes in disks particularly compelling to pursue.

These considerations motivate the search for longer cyanopolyynes in disks. The protoplanetary disk around TW Hya, located at a distance of 60 pc (Gaia Collaboration et al. 2023), provides an exceptional laboratory for such a study. As the nearest T Tauri star, with a stellar mass of 0.88 $M_\odot$ and spectral type K7, TW Hya is often regarded as a close analog to the early solar nebula (e.g., E. A. Bergin et al. 2013). Its bright, nearly face-on disk has been the subject of extensive observational campaigns, yielding detailed constraints on both its dust distribution (e.g., S. M. Andrews et al. 2016; J. Huang et al. 2018) and chemistry (e.g., C. Walsh et al. 2016; C. Favre et al. 2018; R. A. Loomis et al. 2018a; P. Hily-Blant et al. 2019; J. K. Calahan et al. 2021; L. I. Cleeves et al. 2021; K. I. Öberg et al. 2021; J. Terwisscha van Scheltinga et al. 2021).

In this Letter, we present the first detection of HC_5N toward TW Hya. Our observation setup and data reduction are discussed in Section 2. The detection results and a column density analysis are presented in Section 3. In Section 4, we discuss the morphology and formation chemistry of HC_5N. Finally, we summarize our results and implications and outline prospects for future observations.

2. Observations

2.1. Observational Details

TW Hya was observed over seven execution blocks on 2021 March 22, 2021 March 23, 2021 March 25, and 2021 March 28 in Band 3 as part of the ALMA Cycle 6 project 2019.1.00769.S. The total on-source integration time was 325 minutes. The correlator setup was identical for each execution block and included a Time Division Mode (TDM) continuum window centered at 110.169 GHz with a bandwidth of 2GHz as well as a Frequency Division Mode (FDM) spectral windows centered at 99.665, 100.078, 98.541, 96.982, 109.173, and 108.715 GHz. These spectral windows had a bandwidth of 58.594 MHz and channel spacing of 30.518 kHz ($\sim$0.08 km s^{-1}). The main targets of the observations were HC_3N and HC_3N isotopologues, but two transitions of HC_5N were targeted as ancillary bonus lines (see Table 1).

2.2. Calibration and Imaging

The data were initially calibrated by the ALMA Observatory using the ALMA pipeline version 2020.1.0.40 (T. R. Hunter et al. 2023) in CASA 6.1.1.15. The quasar J1037-2934 was used for phase calibration and J1107-4449 was used as the bandpass and flux calibrator across all executions. We then additionally self-calibrated the data with three rounds of phase-only and one round of phase and amplitude self-calibration.

For spectral line imaging, we continuum subtracted the self-calibrated visibilities in the *uv*-plane and CLEANed the lines using natural weighting for maximum sensitivity in CASA 6.1.1.15. This resulted in a beam of $1\farcs07 \times 0\farcs86$ $-84\fdg531$ for the HC_5N $J = 37$–36 transition and $0\farcs97 \times 0\farcs77$ $-85\fdg550$ for the HC_5N $J = 41$–40 and HC_3N $J = 12$–11 transitions, due to their different rest frequencies. These correspond to roughly $\sim$60 au resolution at TW Hya's distance. For HC_3N a Keplerian mask based on the adopted TW Hya disk geometry: $i = 5°$, PA $= 152°$ and system parameters $M_* = 0.88\,M_\odot$, $d = 59.5$ pc, with a radial sampling of $dr = 0.1$ (J. Huang et al. 2018; S. M. Andrews et al. 2012; Gaia Collaboration et al. 2023) was generated for CLEANing, while no mask was used for the HC_5N transitions as there was no significant emission to CLEAN. The achieved rms values were $\sim$1.1 and $\sim$1.3 mJy $\rm bm^{-1}$, respectively, for the $J = 37$–36 and $J = 41$–40 HC_5N transitions and $\sim$1.3 mJy $\rm bm^{-1}$ for HC_3N $J = 12$–11.

3. Results

3.1. HC_3N and HC_5N Integrated Intensity

HC_3N provides a useful reference for our analysis, as it is the only cyanopolyyne previously detected in T Tauri disks (e.g., E. Chapillon et al. 2012; J. B. Bergner et al. 2018; J. D. Ilee et al. 2021; J. K. Calahan et al. 2023) and was the

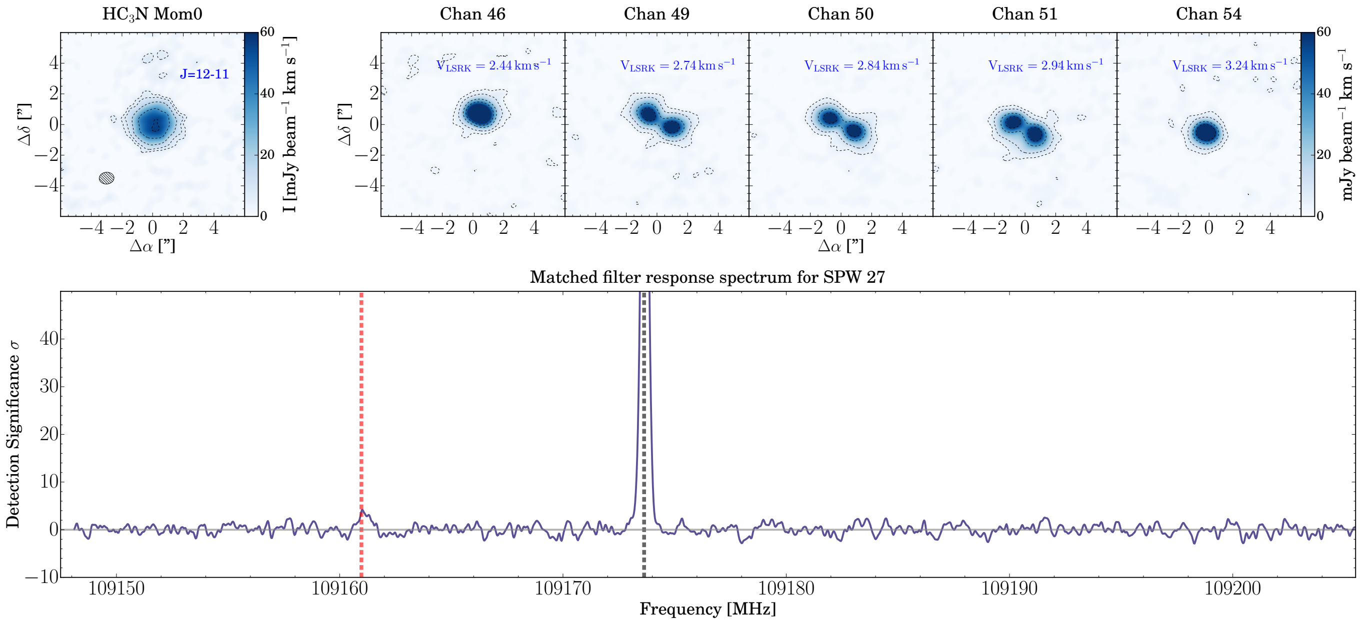

Figure 1. HC_3N J = 12–11 emission. Upper left panel: moment-0 map of HC_3N emission. Top center panels: channel maps of the HC_3N line; selected velocity channels are shown to highlight the Keplerian rotation of the disk. Bottom panel: matched-filter response spectrum for the full spectral window containing the HC_3N J = 12–11 transition. The red dashed line marks the expected rest frequency of HC_5N J = 41–40.

Table 1
Observed Transition Properties

Species	Transition	Frequency[a] (MHz)	E_u (K)	$S_{ij}\mu^2$[b] (D^2)	Int. Flux Dens.[c] (mJy km s^{-1})	Filter Response[d] (σ)
HC_3N	J = 12–11	109173.63	34.05	167.09	275±28	⋯
HC_5N	J = 37–36	98512.524	85.10	2080.91	3.7±3.5	3.4σ
HC_5N	J = 41–40	109160.973	104.78	2305.96	8.3±6.3	4.2σ

Notes.
[a] Center frequency of collapsed hyperfine components (spacing smaller than channel width).
[b] $S_{ij}\mu^2$ of combined hyperfine components.
[c] Velocity-integrated between 2.0–3.7 km s^{-1}.
[d] The HC_3N emission was used as the filter; therefore, a detection significance is not meaningful.

primary target of the observations. Figure 1 (top left) shows a moment-0 map displaying the total integrated intensity of the strongly detected J = 12–11 HC_3N transition. Channel maps (top row) of several select channels show the typical characteristics of Keplerian emission and the overall morphology of the HC_3N within the disk.

Figure 2 (top row) shows the subsequent integrated intensity maps of the two targeted HC_5N lines. These moment maps show no strong signal.

3.2. Matched Filtering Analysis

Given the lack of an obvious image plane detection of the individual HC_5N transitions, we employed a matched filtering technique (e.g., R. A. Loomis et al. 2018b) to enhance line detectability. This approach exploits the fact that HC_5N is expected to trace roughly the same spatiokinematic structure as other species within the disk. We examined multiple filter kernels, all of which had similar results, and thus use here an empirical filter kernel from the strong HC_3N J = 12–11 emission illustrated in Figure 1, with the assumption that HC_3N and HC_5N likely share a similar morphology. This kernel was applied to the observed visibilities across all spectral windows.

Figure 1 (bottom) shows the spectral response function for the full spectral window 27, with an expected strong response for the HC_3N J = 12–11 transition. The figure shows the expected rest frequency of the targeted HC_5N J = 41–40 transition indicated by a dashed red line. This analysis yielded moderately significant responses at the targeted HC_5N frequencies, with individual line significances of 3.4σ and 4.2σ for the J = 37–36 and J = 41–40 transitions, respectively (Figure 2, middle row). A stacked spectrum of the two transitions produces a 5.3σ detection of the species.

3.3. `GoFish` Spectra and Flux Measurements

Having identified these potential weak HC_5N transitions, we next measured their integrated fluxes. We applied the `GoFish` package (R. Teague 2019) to perform a shift and stack analysis (H.-W. Yen et al. 2016), correcting for Keplerian rotation across the disk. The well-established parameters of TW Hya were adopted: inclination $i = 5°$, position angle 152°, distance 60 pc, and stellar mass 0.88 $M_\odot$ (e.g., J. Huang et al. 2018; Gaia Collaboration et al. 2023). Spectra were extracted within

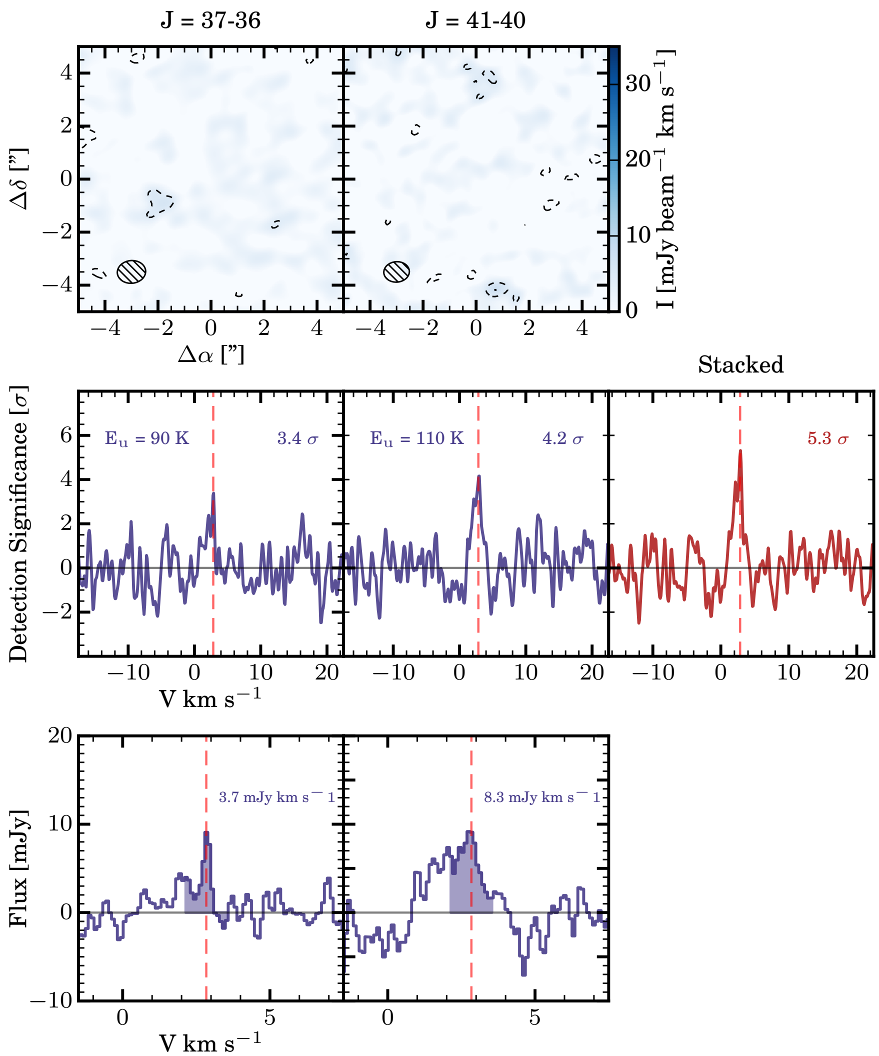

Figure 2. HC_5N emission detected using multiple analysis techniques. Top panels: moment-0 maps of both observed HC_5N transitions. Center panels: matched filtering impulse response spectra of the individual transitions with detection significance labeled (blue), along with the stacked combined spectrum (red). Bottom panels: shifted and stacked image plane spectra for each transition, together with the flux integrated between 2.0 and 3.7 km s^{-1}.

a radius of 90 au, based on the emission extent of HC_3N (Figure 1).

Unlike the matched-filter analysis shown in Figure 2 (middle row), which reports signal to noise in units of significance, the `GoFish` spectra are expressed in flux density (mJy).

`GoFish` analysis of HC3N $J = 12–11$ shows emission from 2.0 to 3.7 km s^{-1}, which is typical of Keplerian emission around TW Hya (J. Huang et al. 2018). Using the same integration range between 2.0 and 3.7 km s^{-1} yields fluxes of 3.7 ± 3.5 mJy km s^{-1} and 8.3 ± 6.3 mJy km s^{-1} for the two HC_5N transitions. This provides the best possible measure of the total flux; however, due to low signal to noise, this alone does not confirm the detection of these transitions.

3.4. Column Density Analysis

These measured fluxes are quite uncertain, but allow us to roughly constrain a disk-averaged column density for different assumed excitation temperatures of HC_5N in TW Hya. Rather than attempting to construct a rotation diagram from two highly uncertain flux values, we opt to directly calculate column densities from the two fluxes and some assumed rotational temperature, and then average them. Following R. A. Loomis et al. (2018a), assuming optically thin emission, we have

$$N_T = \frac{4\pi S_\nu \Delta\nu Q(T_{\rm rot})}{A_{ul}\Omega hcg_u e^{-E_u/kT_{\rm rot}}}, \tag{1}$$

where $S_\nu \Delta\nu$ is the integrated line flux, Ω is the solid angle subtended by the emitting region, A_{ul} is the Einstein A coefficient, $\Delta\nu$ is the line FWHM, E_u and g_u are the upper-state energy and degeneracy, and $Q(T_{\rm rot})$ is the molecular partition function evaluated at the assumed rotational temperature $T_{\rm rot}$.

Using our measured flux estimates from the `GoFish` analysis, we can then estimate column densities of HC_5N for a range of 20–50 K that are reasonable rotational temperatures for Class II T Tauri disks (e.g., Y. Aikawa et al. 2002; K. I. Öberg & E. A. Bergin 2021). The average column density is presented as a range in Table 2, propagating the range of uncertainties from the average measured fluxes of both HC_5N transitions.

We infer a HC_5N column density of $N_T \sim 10^{12}$ cm^{-2} for assumed $T_{\rm rot}$ = 20–50 K. These values are 1 to 2 orders of

Table 2
Derived HC_5N Column Densities

T_{rot} [K]	HC_3N N_T (cm^{-2})	HC_5N N_T (cm^{-2})	Ratio
20	$2.1 \pm 0.2 \times 10^{13}$	$1.3 \pm 1.0 \times 10^{13}$	0.9–7
30	$1.8 \pm 0.2 \times 10^{13}$	$3.4 \pm 2.7 \times 10^{12}$	3–26
40	$1.8 \pm 0.2 \times 10^{13}$	$1.9 \pm 1.5 \times 10^{12}$	5–45
50	$1.9 \pm 0.2 \times 10^{13}$	$1.4 \pm 1.1 \times 10^{12}$	8–63

magnitude lower than typical HC_3N column densities reported for disks (e.g., J. B. Bergner et al. 2018; J. D. Ilee et al. 2021), which is reasonable when comparing to other astronomical regions where cyanopolyynes are detected (e.g., R. A. Loomis et al. 2016). A comparison to predictions of 2D time-dependent chemical models is presented in Section 4.2.

4. Discussion

In this section we examine the formation pathways and expected morphology of HC_5N in TW Hya and compare to a small set of chemical models to further interpret these processes.

4.1. Formation Chemistry and Emission Region of HC_5N

Cyanopolyynes such as HC_5N have long been recognized as key tracers of carbon-chain chemistry, with their formation pathways and physical conditions most clearly established in cold, molecule-rich regions of the ISM. Interpreting the presence of HC_5N in a protoplanetary disk therefore benefits from first considering this broader astrochemical framework. HC_5N was first detected in the ISM toward Sgr B2 (L. W. Avery et al. 1976) and subsequently identified in cold dark clouds in Taurus, most notably TMC-1 (L. T. Little et al. 1977). These clouds served as ideal early laboratories for carbon-chain chemistry because their low temperatures and strong UV shielding allow larger cyanopolyyne species to form efficiently and persist for long timescales. Given these conditions, the dominant formation pathway for cyanopolyynes HC_nN in cold clouds proceeds through gas-phase neutral–neutral reactions of the following general form (K. Fukuzawa et al. 1998):

$$CN + C_{n-1}H_2 \rightarrow HC_{nN} + H. \quad (2)$$

The specific formation pathway for HC_5N is then given by J.-C. Loison et al. (2014):

$$CN + C_4H_2 \rightarrow HC_{5N} + H. \quad (3)$$

Ion–molecule reactions can also contribute to carbon-chain growth in cold, highly ionized gas regions dominated by cosmic rays. In this pathway, hydrocarbon ions react with acetylene to lengthen the carbon backbone, e.g.,

$$C_nH_3^+ + C_2H_2 \rightarrow C_{n+2}H_5^+, \quad (4)$$

after which dissociative recombination produces a longer neutral polyyne,

$$C_{n+2}H_5^+ + e^- \rightarrow C_{n+2}H_2 + H_2 + H. \quad (5)$$

These neutral chains can then react with CN to form the corresponding cyanopolyyne via the reaction shown in Equation (2) providing a secondary formation channel for HC_nN species (e.g., E. Herbst & C. M. Leung 1989; K. Fukuzawa et al. 1998; J.-C. Loison et al. 2014). Any carbon-chain growth on grains is quickly quenched by hydrogenation reactions, making grain surface pathways an inefficient source of HC_5N in cold clouds.

Physical conditions and chemical environments in protoplanetary disks differ substantially from those in cold dark clouds. Temperatures and densities throughout the structure of disks are much higher relative to cold dark clouds, and this simultaneously increases formation rates while promoting adsorption onto grains that hinder survival for carbon chains (K. Fukuzawa et al. 1998). Other destruction pathways arise in disks through their X-ray-induced UV radiation fields that impact the upper layers of the disk, whereas cold dark clouds are shielded from these effects (e.g., E. A. Bergin et al. 2007). This leads to rapid photodissociation of carbon chains in unprotected regions. These unique disk properties additionally affect the abundance of CN (e.g., J. H. Kastner et al. 2014; R. Teague & R. Loomis 2020), which is the precursor to these cyanopolyynes. These X-ray fields as well as the presence of radionuclides give rise to additional mechanisms of ionization that alter the balance of ion–molecule formation pathways in disks (e.g., L. I. Cleeves et al. 2013)

Using the HC_5N/HC_3N column density ratio derived from our analysis in Table 2. Across the assumed range of rotational temperatures, we find that HC_5N is consistently less abundant than HC_3N, with ratios indicating a steep decline in column density with increasing carbon-chain length. This behavior is consistent with that of large carbon chains observed in cold dark cloud environments such as TMC-1 (A. J. Remijan et al. 2006). The similarity in relative abundances suggests that, while disk environments differ markedly in physical conditions from dark clouds, the underlying chemical trend persists in disks. The formation and survival of cyanopolyynes (HC_nN) becomes progressively less efficient as n increases. Our derived ratios therefore support the interpretation that disk chemistry can access long carbon-chain molecules, but with abundances that decline rapidly with molecular size, in line with expectations from both chemical kinetics and observations in other astrophysical environments.

4.2. Comparison of Chemical Models and Observations

To aid interpretation of the observations we ran a small set of disk chemistry models. The two-dimensional time-dependent chemical code used is based on the one from J. K. J. Fogel et al. (2011). The original Ohio State University (OSU) gas-phase network (I. W. M. Smith et al. 2004) was substantially expanded in J. K. J. Fogel et al. (2011) and subsequently further updated to address additional grain surface chemistry, updated photodissociation cross sections, and self-shielding of N_2 (L. I. Cleeves et al. 2014, 2015, 2018) as well as high-temperature gas-phase reactions (D. E. Anderson et al. 2021) and updated sulfur chemistry (B. J. Williams et al. 2025). Additional updates to several binding energies were made and will be described in a forthcoming paper.

The disk physical structure is described using a standard self-similar viscous surface-density prescription, with an exponential taper beyond a characteristic radius R_c of 40 au and a total disk mass of 0.1 $M_\odot$. The high-energy stellar far-UV (FUV) and X-ray radiation field within the disk is calculated using the Monte Carlo code and cross sections from T. J. Bethell & E. A. Bergin (2011); see L. I. Cleeves et al. (2013, 2014) for details. The TW Hya FUV spectrum from

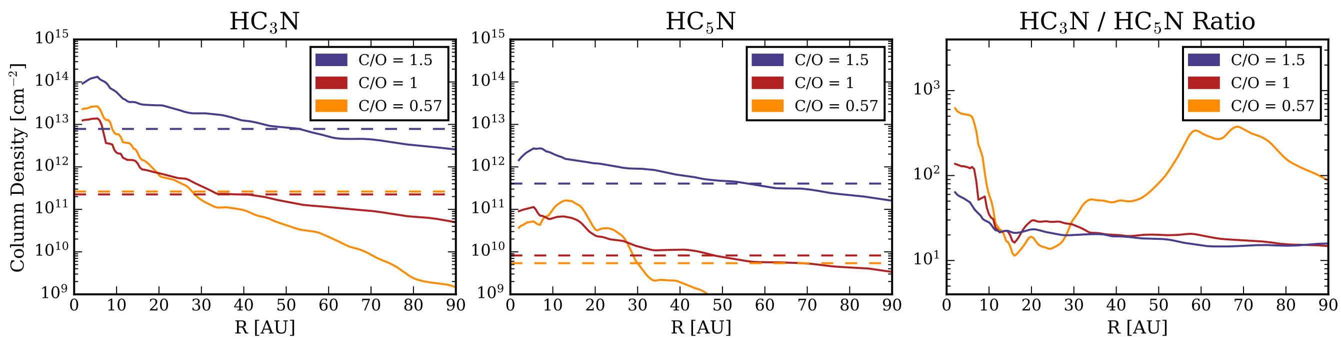

Figure 3. Comparison of HC_3N (left panel) and HC_5N (middle panel) column densities from chemical models assuming different C/O ratios, with dashed lines indicating disk-averaged column densities, and the HC_3N/HC_5N ratio (right panel) for each C/O ratio.

G. J. Herczeg et al. (2002, 2004) and the X-ray spectrum from L. I. Cleeves et al. (2013) are used. We additionally assume a cosmic-ray ionization rate of $\zeta_{CR} = (1.3) \times 10^{-18}$ s^{-1} (L. I. Cleeves et al. 2015). A 90% fraction of large dust grains is assumed, and the model is evolved for 1 Myr.

Three different C/O ratios were considered: 0.57 (solar-like), 1.0, and 1.5. TW Hya shows significant evidence for enhanced C/O ratios in its outer disk (E. A. Bergin et al. 2016; M. Kama et al. 2016; L. I. Cleeves et al. 2021), so we expect the elevated C/O model to more accurately describe our observations. Radial profiles of vertically integrated column densities of HC_3N (left panel) and HC_5N (right panel) from the models are shown in Figure 3. Both show monotonically decreasing column densities with radius and elevated column densities when the C/O ratio is enhanced beyond 1.0, as expected. The HC_3N disk-averaged column density is roughly a few times 10^{13} cm^{-2}, in line with our observations, while the HC_5N disk-averaged column density is $\sim 10^{12}$ cm^{-2}. This value is in moderate agreement with our estimated column density, especially with a higher assumed rotational temperature of $\geqslant$30 K, as might be expected for formation in the higher disk layers. For both HC_3N and HC_5N, the inner 10 au shows enhanced formation, but we caution that interpretation of these regions of the disk may be difficult both due to model resolution as well as proposed C/O depletion in the inner TW Hya disk (A. D. Bosman & A. Banzatti 2019). More realistic modeled column density profiles may then look like a hybrid of the models presented here, transitioning between them at a radius of 5–30 au.

5. Summary

We have reported the first detection of HC_5N toward the TW Hya protoplanetary disk, representing the largest cyanopolyyne identified to date in a Class II system. We tentatively detected two individual HC_5N transitions in ALMA Band 3 with a 5.3σ stacked detection and derived a beam-averaged column density $N_T \sim 10^{12}\,\mathrm{cm}^{-2}$ with assumed excitation temperatures between 20 and 50 K. Although our observations do not resolve any radial or vertical structure, known HC_5N chemistry in molecular clouds indicates that HC_5N should arise in a region where CN and small hydrocarbons coexist. A simple chemical model supports this interpretation, predicting column densities consistent with the observed values and requiring elevated C/O ratios (consistent with previous studies of TW Hya) for HC_5N to reach detectable levels. Together, these results extend the known carbon-chain inventory of Class II disks and provide new constraints on nitrogen-bearing chemistry in planet-forming environments.

Acknowledgments

The National Radio Astronomy Observatory is a facility of the National Science Foundation operated under cooperative agreement by Associated Universities, Inc. This Letter makes use of the following ALMA data: ADS/JAO.ALMA #2019.1.00769.S. ALMA is a partnership of ESO (representing its member states), NSF (USA) and NINS (Japan), together with NRC (Canada) and NSC and ASIAA (Taiwan), in cooperation with the Republic of Chile. The Joint ALMA Observatory is operated by ESO, AUI/NRAO and NAOJ.

L.I.C. also acknowledges support from the Research Corporation for Science Advancement Cottrell Scholarship Award 28249, the David and Lucille Packard Foundation, and NSF AAG Awards 2205698 and 2407547.

Support for C.J.L. was provided by NASA through the NASA Hubble Fellowship grant No. HST-HF2-51535.001-A awarded by the Space Telescope Science Institute, which is operated by the Association of Universities for Research in Astronomy, Inc., for NASA, under contract NAS5-26555.

A.D. acknowledges support from the NASA FINESST grant No. 80NSSC24K1470 and the ACM SIGHPC Computational and Data Science Fellowship.

V.V.G. acknowledges support from the ANID—Millennium Science Initiative Program—Center Code NCN2024_001, from FONDECYT Regular 1221352, and ANID CATA-BASAL project FB210003.

Y.A. acknowledges support from JSPS KAKENHI Grant Number 24K00674.

This work made use of the ChatGPT large language model (OpenAI) for limited assistance with text editing and code formatting.

Software: Astropy (Astropy Collaboration et al. 2013, 2018, 2022), CASA (CASA Team et al. 2022), `GoFish` (R. Teague 2019), Matplotlib (J. D. Hunter 2007), NumPy (C. R. Harris et al. 2020), VISIBLE (R. A. Loomis et al. 2018b), ChatGPT 5.1 (OpenAI 2025).

ORCID iDs

Ryan A. Loomis https://orcid.org/0000-0002-8932-1219
Amina Diop https://orcid.org/0009-0006-0491-6210
L. Ilsedore Cleeves https://orcid.org/0000-0003-2076-8001
Yuri Aikawa https://orcid.org/0000-0003-3283-6884
Romane Le Gal https://orcid.org/0000-0003-1837-3772
Karin Oberg https://orcid.org/0000-0001-8798-1347

Richard Teague https://orcid.org/0000-0003-1534-5186
Catherine Walsh https://orcid.org/0000-0001-6078-786X

References

Aikawa, Y., Okuzumi, S., & Pontoppidan, K. 2024, in in Comets III, ed. K. J. Meech et al. (Univ. Arizona Press), 33
Aikawa, Y., van Zadelhoff, G. J., van Dishoeck, E. F., & Herbst, E. 2002, A&A, 386, 622
Akeson, R. L., Chen, X., Ciardi, D., et al. 2013, PASP, 125, 989
Anderson, D. E., Blake, G. A., Cleeves, L. I., et al. 2021, ApJ, 909, 55
Andrews, S. M., Wilner, D. J., Hughes, A. M., et al. 2012, ApJ, 744, 162
Andrews, S. M., Wilner, D. J., Zhu, Z., et al. 2016, ApJL, 820, L40
Astropy Collaboration, Price-Whelan, A. M., Lim, P. L., et al. 2022, ApJ, 935, 167
Astropy Collaboration, Price-Whelan, A. M., Sipőcz, B. M., et al. 2018, AJ, 156, 123
Astropy Collaboration, Robitaille, T. P., Tollerud, E. J., et al. 2013, A&A, 558, A33
Avery, L. W., Broten, N. W., MacLeod, J. M., Oka, T., & Kroto, H. W. 1976, ApJL, 205, L173
Bergin, E. A., Aikawa, Y., Blake, G. A., & van Dishoeck, E. F. 2007, Protostars and Planets V (Univ. Arizona Press), 751
Bergin, E. A., Cleeves, L. I., Gorti, U., et al. 2013, Natur, 493, 644
Bergin, E. A., Du, F., Cleeves, L. I., et al. 2016, ApJ, 831, 101
Bergner, J. B., Guzmán, V. G., Öberg, K. I., Loomis, R. A., & Pegues, J. 2018, ApJ, 857, 69
Bergner, J. B., Öberg, K. I., Guzmán, V. V., et al. 2021, ApJS, 257, 11
Bethell, T. J., & Bergin, E. A. 2011, ApJ, 739, 78
Booth, A. S., Calahan, J., Temmink, M., et al. 2026, AJ, 171, 128
Booth, A. S., Temmink, M., van Dishoeck, E. F., et al. 2024, AJ, 167, 165
Booth, A. S., Wölfer, L., Temmink, M., et al. 2025, ApJL, 986, L9
Bosman, A. D., & Banzatti, A. 2019, A&A, 632, L10
Broten, N. W., Oka, T., Avery, L. W., MacLeod, J. M., & Kroto, H. W. 1978, ApJL, 223, L105
Burkhardt, A. M., Herbst, E., Kalenskii, S. V., et al. 2018, MNRAS, 474, 5068
Calahan, J. K., Bergin, E., Zhang, K., et al. 2021, ApJ, 908, 8
Calahan, J. K., Bergin, E. A., Bosman, A. D., et al. 2023, NatAs, 7, 49
Carr, J. S., & Najita, J. R. 2008, Sci, 319, 1504
CASA Team, Bean, B., Bhatnagar, S., et al. 2022, PASP, 134, 114501
Cataldi, G., Yamato, Y., Aikawa, Y., et al. 2021, ApJS, 257, 10
Chapillon, E., Dutrey, A., Guilloteau, S., et al. 2012, ApJ, 756, 58
Cleeves, L. I., Adams, F. C., & Bergin, E. A. 2013, ApJ, 772, 5
Cleeves, L. I., Bergin, E. A., & Adams, F. C. 2014, ApJ, 794, 123
Cleeves, L. I., Bergin, E. A., Qi, C., Adams, F. C., & Öberg, K. I. 2015, ApJ, 799, 204
Cleeves, L. I., Öberg, K. I., Wilner, D. J., et al. 2018, ApJ, 865, 155
Cleeves, L. I., Loomis, R. A., Teague, R., et al. 2021, ApJ, 911, 29
Dutrey, A., Guilloteau, S., & Guelin, M. 1997, A&A, 317, L55
Favre, C., Fedele, D., Semenov, D., et al. 2018, ApJL, 862, L2
Fogel, J. K. J., Bethell, T. J., Bergin, E. A., Calvet, N., & Semenov, D. 2011, ApJ, 726, 29
Fukuzawa, K., Osamura, Y., & Schaefer, H. F., III 1998, ApJ, 505, 278
Gaia Collaboration, Vallenari, A., Brown, A. G. A., et al. 2023, A&A, 674, A1
Gibb, E. L., Van Brunt, K. A., Brittain, S. D., & Rettig, T. W. 2007, ApJ, 660, 1572
Guzmán, V. V., Öberg, K. I., Huang, J., Loomis, R., & Qi, C. 2017, ApJ, 836, 30
Harris, C. R., Millman, K. J., van der Walt, S. J., et al. 2020, Natur, 585, 357
Herbst, E., & Leung, C. M. 1989, ApJS, 69, 271
Herczeg, G. J., Linsky, J. L., Valenti, J. A., Johns-Krull, C. M., & Wood, B. E. 2002, ApJ, 572, 310
Herczeg, G. J., Wood, B. E., Linsky, J. L., Valenti, J. A., & Johns-Krull, C. M. 2004, ApJ, 607, 369
Hily-Blant, P., Magalhaes de Souza, V., Kastner, J., & Forveille, T. 2019, A&A, 632, L12
Huang, J., Andrews, S. M., Cleeves, L. I., et al. 2018, ApJ, 852, 122
Hunter, J. D. 2007, CSE, 9, 90
Hunter, T. R., Indebetouw, R., Brogan, C. L., et al. 2023, PASP, 135, 074501
Ilee, J. D., Walsh, C., Booth, A. S., et al. 2021, ApJS, 257, 9
Jørgensen, J. K., van der Wiel, M. H. D., Coutens, A., et al. 2016, A&A, 595, A117
Kama, M., Bruderer, S., Carney, M., et al. 2016, A&A, 588, A108
Kastner, J. H., Hily-Blant, P., Rodriguez, D. R., Punzi, K., & Forveille, T. 2014, ApJ, 793, 55
Kastner, J. H., Zuckerman, B., Weintraub, D. A., & Forveille, T. 1997, Sci, 277, 67
Le Roy, L., Altwegg, K., Balsiger, H., et al. 2015, A&A, 583, A1
Little, L. T., Riley, P. W., & Matheson, D. N. 1977, MNRAS, 181, 33P
Loison, J.-C., Wakelam, V., & Hickson, K. 2014, MNRAS, 443, 398
Loomis, R. A., Burkhardt, A. M., Shingledecker, C. N., et al. 2021, NatAs, 5, 188
Loomis, R. A., Cleeves, L. I., Öberg, K. I., et al. 2018a, ApJ, 859, 131
Loomis, R. A., Öberg, K. I., Andrews, S. M., et al. 2018b, AJ, 155, 182
Loomis, R. A., Shingledecker, C. N., Langston, G., et al. 2016, MNRAS, 463, 4175
Murillo, N. M., van Dishoeck, E. F., Hacar, A., Harsono, D., & Jørgensen, J. K. 2022, A&A, 658, A53
Öberg, K. I., & Bergin, E. A. 2021, PhR, 893, 1
Öberg, K. I., Cleeves, L. I., Bergner, J. B., et al. 2021, AJ, 161, 38
Öberg, K. I., Guzmán, V. V., Furuya, K., et al. 2015, Natur, 520, 198
Öberg, K. I., Facchini, S., & Anderson, D. E. 2023, ARA&A, 61, 287
Öberg, K. I., Qi, C., Fogel, J. K. J., et al. 2011, ApJ, 734, 98
OpenAI 2025, Large Language Model Used for Language Editing and Drafting Assistance, ChatGPT 5.1, https://chat.openai.com/
Paneque-Carreño, T., Izquierdo, A. F., Teague, R., et al. 2024, A&A, 684, A174
Phuong, N. T., Dutrey, A., Chapillon, E., et al. 2021, A&A, 653, L5
Powner, M. W., Gerland, B., & Sutherland, J. D. 2009, Natur, 459, 239
Remijan, A. J., Hollis, J. M., Snyder, L. E., Jewell, P. R., & Lovas, F. J. 2006, ApJL, 643, L37
Sakai, N., Sakai, T., Hirota, T., & Yamamoto, S. 2011, EAS, 52, 235
Smith, I. W. M., Herbst, E., & Chang, Q. 2004, MNRAS, 350, 323
Taniguchi, K., Herbst, E., Caselli, P., et al. 2019, ApJ, 881, 57
Taniguchi, K., Saito, M., Hirota, T., et al. 2017, ApJ, 844, 68
Teague, R. 2019, JOSS, 4, 1632
Teague, R., Guilloteau, S., Semenov, D., et al. 2016, A&A, 592, A49
Teague, R., Lankhaar, B., Andrews, S. M., et al. 2025, ApJL, 991, L6
Teague, R., & Loomis, R. 2020, ApJ, 899, 157
Terwisscha van Scheltinga, J., Hogerheijde, M. R., Cleeves, L. I., et al. 2021, ApJ, 906, 111
Thi, W.-F., van Zadelhoff, G.-J., & van Dishoeck, E. F. 2004, A&A, 425, 955
van Zadelhoff, G.-J., van Dishoeck, E. F., Thi, W.-F., & Blake, G. A. 2001, A&A, 377, 566
Walsh, C., Loomis, R. A., Öberg, K. I., et al. 2016, ApJL, 823, L10
Walsh, C., Millar, T. J., Nomura, H., et al. 2014, A&A, 563, A33
Williams, B. J., Cleeves, L. I., Gross, R. E., & Baker, J. 2025, ApJ, 992, 202
Yamato, Y., Aikawa, Y., Guzmán, V. V., et al. 2024, ApJ, 974, 83
Yen, H.-W., Koch, P. M., Liu, H. B., et al. 2016, ApJ, 832, 204
Zahnle, K. J. 1986, JGRD, 91, 2819